Particle production at very low transverse momenta in Au+Au collisions at $\sqrt{s_{NN}} = 200$ GeV

B.B.Back[1], M.D.Baker[2], M.Ballintijn[4], D.S.Barton[2], R.R.Betts[6], A.A.Bickley[7], R.Bindel[7], A.Budzanowski[3], W.Busza[4], A.Carroll[2], M.P.Decowski[4], E.García[6], N.George[1,2], K.Gulbrandsen[4], S.Gushue[2], C.Halliwell[6], J.Hamblen[8], G.A.Heintzelman[2], C.Henderson[4], D.J.Hofman[6], R.S.Hollis[6], R.Hołyński[3], B.Holzman[2], A.Iordanova[6], E.Johnson[8], J.L.Kane[4], J.Katzy[4,6], N.Khan[8], W.Kucewicz[6], P.Kulinich[4], C.M.Kuo[5], W.T.Lin[5], S.Manly[8], D.McLeod[6], A.C.Mignerey[7], R.Nouicer[6], A.Olszewski[3], R.Pak[2], I.C.Park[8], H.Pernegger[4], C.Reed[4], L.P.Remsberg[2], M.Reuter[6], C.Roland[4], G.Roland[4], L.Rosenberg[4], J.Sagerer[6], P.Sarin[4], P.Sawicki[3], W.Skulski[8], S.G.Steadman[4], P.Steinberg[2], G.S.F.Stephans[4], A.Sukhanov[2], J.-L.Tang[5], A.Trzupek[3], C.Vale[4], G.J.van Nieuwenhuizen[4], R.Verdier[4], F.L.H.Wolfs[8], B.Wosiek[3], K.Woźniak[3], A.H.Wuosmaa[1], B.Wysłouch[4]

[1] Argonne National Laboratory, Argonne, IL 60439-4843, USA
[2] Brookhaven National Laboratory, Upton, NY 11973-5000, USA
[3] Institute of Nuclear Physics PAN, Kraków, Poland
[4] Massachusetts Institute of Technology, Cambridge, MA 02139-4307, USA
[5] National Central University, Chung-Li, Taiwan
[6] University of Illinois at Chicago, Chicago, IL 60607-7059, USA
[7] University of Maryland, College Park, MD 20742, USA
[8] University of Rochester, Rochester, NY 14627, USA
(Dated: October 21, 2004)

We present results on charged particle production at very low transverse momenta in the 15% most central Au+Au collisions at $\sqrt{s_{NN}} = 200$ GeV obtained with the PHOBOS detector at RHIC. The invariant yields were measured at mid-rapidity in the transverse momentum ranges from 30 to 50 MeV/c for charged pions, 90 to 130 MeV/c for charged kaons and 140 to 210 MeV/c for protons and antiprotons. No significant enhancement in low transverse momentum particle production is observed as compared to extrapolations of identified particle spectra measured at an intermediate p_T range. The spectra tend to flatten at low p_T, consistent with the expectations of transverse expansion of the system.

PACS numbers: 25.75.-q

Collisions of gold nuclei at the Relativistic Heavy Ion Collider (RHIC) provide the means to study strongly interacting matter under conditions of high temperature and energy density. The study of low-p_T particle production is particularly interesting as it is directly associated with the long-distance scales, accessible in heavy ion collisions but out of reach in hadronic interactions. Any enhancement of the low-p_T yields compared to extrapolations from higher transverse momenta could indicate interesting effects, e.g. new long-wavelength physics phenomena [1]. Pion production may also be modified if a transient state with partially restored chiral symmetry is produced in the early stage of the collision [2–4].

The spectra of identified hadrons measured at RHIC at $\sqrt{s_{NN}} = 200$ GeV [5–7] tend to flatten in the low p_T region. This effect is more pronounced for heavier particles and is commonly attributed to a collective transverse expansion of the system. Hydrodynamics-based models incorporating transverse expansion provide a satisfactory description of the spectra measured above 0.2 GeV/c [8–10]. Other mechanisms, such as initial state parton interactions [11, 12] or final state hadron reinteractions, can also describe the broadening of the spectra and an increase of $\langle p_T \rangle$ with particle mass. Still, if transverse flow develops during the evolution of the system produced in heavy ion collisions, the effects of flow would likely be observed at very low p_T.

In this paper we present data on particle production at very low transverse momenta, $p_T < 0.2$ GeV/c, a region thus far not explored at RHIC energies. The PHOBOS detector at RHIC has the unique capability to detect particles with very low p_T in the two-arm spectrometer [13]. Each spectrometer arm consists of 16 layers of Si detectors. The six innermost layers are located in an approximately field-free region near the beam pipe. The proximity of the sensitive detector layers to the interaction region, the small amount of material between the collision vertex and the Si layers, and the high segmentation of the Si detectors permit a precise measurement of particles with small p_T.

The data were taken during the 2001 RHIC run. The event triggering, determination of the collision centrality and the position of the collision vertex were as described in [13, 14]. For this analysis we selected the 15% most central Au+Au collisions ($\langle N_{part} \rangle = 303$, where N_{part} is the number of participating nucleons). Events with the reconstructed vertex position along the beam axis between -7 cm and +14 cm, relative to the nominal interaction point were accepted. The centrality and vertex selections yielded 2×10^6 events.

In this analysis we searched for particles stopped in the 5^{th} spectrometer layer. The reconstruction of particle trajectories and determination of the particle mass was based on a detailed analysis of the measured energy depositions in the first five spectrometer layers. Selection criteria based on the energy depositions [15] for track candidates were derived from an analysis of single stopping particles obtained from GEANT simulations of the PHOBOS detector [16]. Initially, all possible 5-hit track candidates were formed from hits with large energy depositions ($dE/dx > 0.5$ MeV normalized to $300\mu m$ of Si, roughly 6 times the deposition of a minimum ionizing particle). For the kinetic energies of particles stopping in the 5^{th} layer (about 8 MeV for pions, 19 MeV for kaons and 21 MeV for protons) the energy losses depend on the particle mass [17, 18] as shown in the inset in Fig. 1. Each track candidate satisfied the requirement $|(dE/dx)_i - < dE/dx >_i | < 1.4\sigma_i$, $i = 1, ..., 4$, where the mean and the rms value σ_i, are calculated from the $(dE/dx)_i$ distributions for single simulated stopping particles.

A mass parameter was defined as $(M_p)_i = (dE/dx)_i \sum_{k=i}^{5} E_k$, for the first four layers, where E_k denotes the energy deposited in the k^{th} layer. For non-relativistic particles, the mass parameter $(M_p)_i$ depends only on the particle mass, since $(dE/dx)_i \sim 1/\beta^2$ and $\sum_{k=i}^{5} E_k \sim m\beta^2/2$. Since the measured energy deposition in the fifth layer (E_5) cannot be used, due to contributions from annihilation and decay products, we estimated E_5 using the properties of the mass parameter and the assumption that the particle stops in the 5^{th} layer. Having estimated E_5 we calculate the average mass parameter, M_p, and the total deposited energy, $E_{tot} = \sum_{i=1}^{5} E_i$. Fig. 1 shows a scatter plot of M_p vs. E_{tot}, for track candidates found in the data which satisfy the selection criteria on dE/dx in the first four Si layers.

The momenta of stopped particles are restricted by imposing cuts on E_{tot} (see Fig. 1). For track candidates with emission angles smaller than 60^o, not shown in Fig. 1, about 10% higher upper limits on E_{tot} were applied as compared to those shown in Fig. 1. Additional cuts on the angular deviations of the candidate track from a straight-line trajectory were imposed to reject false tracks. The cuts are mass dependent to account for differences in the multiple scattering of low-momentum pions, kaons and protons. This analysis procedure was tested on samples of simulated low-momentum charged particles. Reconstructed single tracks simulated by GEANT were used to calibrate the final particle momenta. The transverse momentum resolution is estimated to be approximately 5%. These measurements are confined to the mid-rapidity region ($-0.1 < y < 0.4$) and cover a limited range of transverse momenta: 30 to 50 MeV/c for charged pions, 90 to 130 MeV/c for charged kaons and 140 to 210 MeV/c for protons and antiprotons.

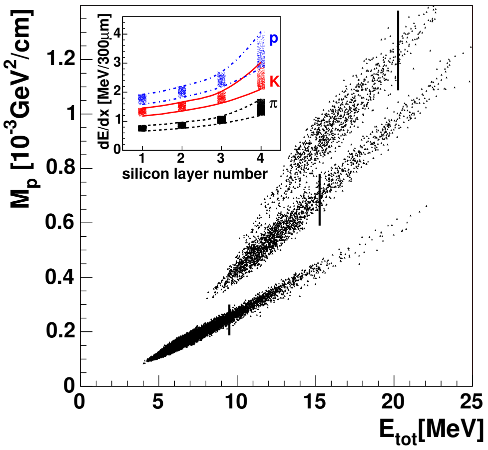

FIG. 1: (Color online) (M_p, E_{tot}) scatter plot for the candidate tracks after the $(dE/dx)_i$ cuts in the first four spectrometer layers. Only track candidates with emission angles larger than 60^o are shown. The upper limits on E_{tot} are marked by vertical lines. An inset shows 1σ bands on the specific energy loss in the first four Si layers for simulated particles.

For further analysis the reconstructed particles were divided into narrow $(\Delta y, \Delta p_T)$ bins. For each bin, corrections were applied to the raw yields to account for acceptance, reconstruction and particle identification inefficiencies, and absorption in the beam pipe. These corrections were obtained by embedding simulated low-momentum particle tracks into real data events, and range between 0.2 and 0.7%.

The acceptance and efficiency corrected particle yields are contaminated by various background contributions: feed-down from weak decays and contributions from secondary, misidentified and ghost particles. For protons and antiprotons the dominant background contributions originate from secondary particles produced in the beam pipe or detector material and products from weak decays. To estimate the background contamination of the $(p + \overline{p})$ yields, we analyzed the distributions of the measured distance of closest approach (DCA) from the vertex position to the particle trajectory, determined by a straight line passing through the hits in the first and third spectrometer layers. The experimental DCA distribution is broader and has a tail to larger DCA values compared to the same distribution for reconstructed primary proton tracks. Parameterized shapes of the DCA distributions for reconstructed primary, secondary and feed-down protons, obtained from an analysis of HIJING events [19], were used to describe the measured DCA spectrum. An example of the fit, assuming equal weights of the two background components, is shown in Fig. 2. The fitted fraction of background particles, averaged over all possible weights for the two background components amounts to $0.31 \pm 0.04(stat.) \pm 0.19(syst.)$. The large systematic

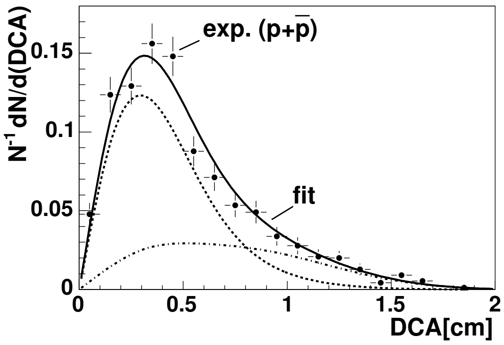

FIG. 2: DCA distribution for reconstructed proton tracks in the data sample (points with error bars). The result of the fit to the measured distribution (see text for more explanations) is denoted by the solid curve. The dashed (dashed-dotted) curve shows the contribution from primary (background) particles.

error assigned to this fraction reflects the dependence of the total background estimate on the relative importance of secondary and feed-down contributions. The fraction of background particles thus determined agrees with the estimate of 0.34 ± 0.03, obtained directly from the reconstruction of HIJING events.

To estimate the background corrections for kaons and pions we used HIJING simulations with yields tuned to account for the fact that HIJING overpredicts the yields of different particle species [20]. This adjustment of HIJING yields is important for evaluating the background correction for charged kaons which is dominated by misidentified protons. The estimated background in the measured kaon sample is 0.10 ± 0.04, while the background level in the unscaled HIJING events is higher (0.23 ± 0.03) due to the larger relative yield of protons to kaons. For protons and kaons the corrections are averaged over the full p_T range.

The charged pion background estimates for scaled and unscaled HIJING events agree. In this case, feed-down from weak decays and ghost tracks are the main source of the background contamination. The large number of reconstructed pions in the simulated events permit the determination of the p_T dependence of the background corrections, which varies between 0.31 ± 0.04 and 0.22 ± 0.02 for p_T of 0.03 GeV/c to 0.05 GeV/c.

The relative statistical uncertainties from the data as well as the statistical errors on the acceptance, efficiency and background corrections are 4 % for $\pi^{\pm}$, 10 % for $K^{\pm}$ and 12 % for $(p+\overline{p})$. Various sources of systematic errors were investigated, related to the backgrounds, the analysis method, and detector effects. Table I summarizes the final estimates of the systematic uncertainties.

The dominant contribution to the systematic errors is due to the uncertainty in the background estimates which are evaluated to be approximately 28% for $(p+\overline{p})$ and about 10% for charged pions and kaons.

TABLE I: The estimated systematic errors (%) on the measured invariant yields.

Source	$\pi^+ + \pi^-$	$K^+ + K^-$	$p + \overline{p}$
Method	7.5	12.1	13.5
Detector	3.8	7.7	9.9
Background	9.0	10.0	27.5

The uncertainties related to the analysis method were estimated by performing the reconstruction with varied selection criteria. There are also contributions estimated by the reconstruction of HIJING events, and of events which were generated with p_T spectra approximately consistent with our measured data and with intermediat-p_T results from other experiments [5–7]. In addition, a 5% uncertainty in the p_T scale and the sensitivity to the GEANT energy threshold contribute to the systematic uncertainty of the reconstruction method.

The dominant contributions to the detector-related error come from the differences in particle yields measured separately in the two spectrometer arms and under different magnetic field polarities, and the calibration of energy depositions. Other detector effects such as misalignment of the spectrometer layers, and the accuracy of the vertex position, were found to be negligible.

The individual contributions from different sources of systematic uncertainty are added in quadrature to derive the total systematic error for these measurements: 12% for $\pi^{\pm}$, 18% for $K^{\pm}$ and 32% for $(p+\overline{p})$.

The fully corrected invariant yields, $(2\pi p_T)^{-1} d^2N/dp_T dy$, of charged particles produced in the 15% most central Au+Au collisions at $\sqrt{s_{NN}} =$ 200 GeV are shown in Fig. 3, together with the yields of identified hadrons measured by PHENIX [6] for the same centrality selection. Different parameterizations have been used to extrapolate the measurements at higher p_T to $p_T \approx 0$ in order to determine the mean p_T and integrated particle yields [5–7]. Measurements at very low p_T provide some constraints on the choice of the functional form which fits the p_T spectra. The functional form $A[exp(m_T/T_{fit})+\epsilon]^{-1}$, with $\epsilon = -1(+1)$ for mesons (baryons), reasonably well describes the intermediate-p_T PHENIX measurements ($m_T - m_h \leq 1\ GeV/c^2$). The fit parameter, T_{fit}, equals 0.229 ± 0.005, 0.293 ± 0.01 and $0.392 \pm 0.015\ GeV/c^2$ correspondingly for charged pions, kaons and $(p+\overline{p})$. An extrapolation of the fits to low p_T agrees with the measured low-p_T yields (see Fig. 3).

It was predicted that the m_T spectra of different particle species should follow a universal function of m_T [11, 12]. One implication of the m_T scaling described in [12] is that the spectral shapes should be independent of particle mass over a wide range of m_T. In Fig. 4 the yields normalized at $m_T = 2\ GeV/c^2$ are shown as a function of m_T. This choice of normalization was mo-

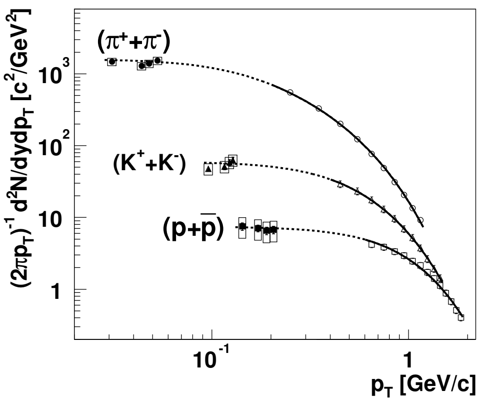

FIG. 3: Invariant yields as a function of p_T. For low-p_T yields (closed symbols) the boxes show systematic uncertainties. For comparison the intermediate-p_T measurements from PHENIX [6] are depicted by open symbols. The fits to PHENIX measurements (solid curves) are extrapolated to low p_T (dashed curves). See text for more details.

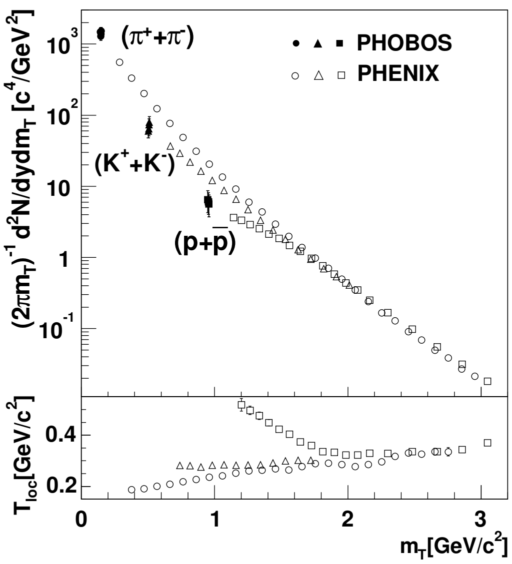

FIG. 4: Invariant yields, normalized at $m_T = 2GeV/c^2$, as a function of m_T. Lower panel shows the m_T dependence of the local inverse slopes.

tivated by an analysis of the local inverse slopes, T_{loc}, obtained from the exponential fits done with a sliding window enclosing 5 consecutive m_T points. (The first inverse slope is from the fit to our average yield and the first four PHENIX points.) As illustrated in the lower panel of Fig. 4, these local inverse slopes converge at $m_T \approx 2\ GeV/c^2$. The normalized m_T spectra are consistent with the scaling hypothesis in the range of m_T from about 1.5 to 2.2 GeV/c^2. However at low m_T, close to the threshold, the spectra for heavier particles deviate from the charged pion spectrum, with larger deviations observed for the $(p+\overline{p})$ yields than for the charged kaons. This observation is consistent with mass dependent flattening of the spectra at low m_T, expected in the presence of transverse expansion of the system, and contradicts the suggested m_T scaling [12].

Effects of the collective transverse expansion are naturally accounted for in the description of the system evolution based on hydrodynamic calculations. A hydrodynamic description within the framework of the single-freeze-out model [8] tends to overestimate the spectra of protons and anti-protons measured at low p_T in central Au+Au collisions. On the other hand, it was shown, within another hydrodynamic approach [9], that the measured spectra at low p_T can be reasonably reproduced only after inclusion of an initial pre-equilibrium transverse expansion.

In summary, the yields of identified particles have been measured at very low p_T (below 210 MeV/c) in central $\sqrt{s_{NN}} = 200$ GeV Au+Au collisions. We see no enhancement in the production of particles with very low transverse momenta, which might have indicated the presence of unusual long-wavelength phenomena. The low-p_T yields agree with extrapolations from intermediate-p_T measurements. Finally, the measurements in this region of phase space, unexplored until now, show clear flattening of particle spectra that increases with particle mass. This observation supports an interpretation of the data in terms of a collective transverse expansion of the system and is consistent with the strongly-interacting nature of the medium created in the collision.

This work was partially supported by U.S. DOE grants DE-AC02-98CH10886, DE-FG02-93ER40802, DE-FC02-94ER40818, DE-FG02-94ER40865, DE-FG02-99ER41099, and W-31-109-ENG-38 as well as NSF grants 9603486, 9722606 and 0072204. The Polish group was partially supported by KBN grant 1-P03B-062-27. The NCU group was partially supported by NSC of Taiwan under contract NSC 89-2112-M-008-024.

[1] W. Busza, *Particle Production in Highly Excited Matter* (Plenum Press, New York, 1993), p. 149.
[2] J. P. Blaizot and A. Krzywicki, Acta Phys. Pol. **B27**, 1687 (1996).
[3] J. Bjorken, Acta Phys. Pol. **B28**, 2773 (1997).
[4] T. Petersen and J. Randrup, Phys. Rev. **C61**, 024906 (2000).
[5] J. Adams et al., Phys. Rev. Lett. **92**, 112301 (2004).
[6] S. S. Adler et al., Phys. Rev. **C69**, 034909 (2004).
[7] I. G. Bearden et al., Nucl. Phys. **A715**, 171c (2003), arXiv:nucl-ex/0403050.
[8] A. Baran, W. Broniowski, and W. Florkowski, Acta Phys. Pol. **B35**, 779 (2004).
[9] P. Kolb and R. Rapp, Phys. Rev. **C67**, 044903 (2003).
[10] U. Heinz and P. Kolb, Nucl. Phys. **A702**, 269 (2002).
[11] M. A. Braun, F. del Moral, and C. Pajares Nucl. Phys. **A715**, 791c (2003).

[12] J. Schaffner-Bielich, D. Kharzeev, L. McLerran, and R. Venugopalan, Nucl. Phys. **A705**, 494 (2002), arXiv:nucl-th/0202054.
[13] B. B. Back et al., Nucl. Inst. Meth. **A499**, 603 (2003).
[14] B. B. Back et al., Phys. Rev. **C65**, 061901(R) (2002).
[15] H. Pernegger et al., Nucl. Inst. Meth. **A473**, 197 (2001).
[16] GEANT 3.2.1, CERN Program Library.
[17] K. Hagiwara et al. (Particle Data Group), Phys. Rev. **D66**, 010001 (2002).
[18] W. R. Leo, *Techniques for Nuclear and Particle Physics Experiments* (Springer, Berlin. Germany, 1987), p. 368.
[19] M. Gyulassy and X. Wang, Phys. Rev. **D44**, 3501 (1991).
[20] B. Wosiek et al., Nucl. Phys. **A715**, 510c (2003).